In Situ Detection of α-Synuclein Seeding Activity Using Quiescent Seed Amplification Assay

Hengxu Mao[1, #], Yaoyun Kuang[1, #], Wei Dai[2], Hao Lin[1] and Ping-Yi Xu[1, *]

Author affiliations:

1. Dept. of Neurology, the First Affiliated Hospital of Guangzhou Medical University, Guangzhou, 510120, China.

2. Graduate School, Xinjiang Medical University, Urumqi, 830054, China

[#]These authors are equally contributing to this work.

***Corresponding to:**

1. Ping-Yi Xu, Dept. of Neurology, the First Affiliated Hospital of Guangzhou Medical University, Guangzhou, 510120, China. Email address: pingyixu@sina.com.

Abstract

Accurate detection of α-synuclein (αSyn) seeding activity is crucial for understanding synucleinopathies like Parkinson's disease. Traditional seed amplification assays lack spatial resolution, while antibody-based methods only capture pre-formed aggregates. To overcome this limitation, we developed the Quiescent Seed Amplification Assay (QSAA), enabling the *in situ* amplification and visualization of αSyn seeding activity directly within tissue sections. Using QSAA, we generated the first brain-wide map of seeding activity in mice injected with αSyn pre-formed fibrils and identified endogenous αSyn aggregates in human brain samples. Additionally, by combined QSAA with immunofluorescence, IF-QSAA revealed that a portion of αSyn seeding occurs independently of pathological aggregates detected by antibodies, such as pS129. This highlights the complementary value of seeding activity mapping alongside antibody-based assessments of Lewy body pathology. Overall, QSAA and IF-QSAA provide valuable tools for investigating αSyn seeding and propagation, offering new insights into synucleinopathy pathogenesis and potential therapeutic strategies.

Keywords: α-Synuclein, Seed amplification assay, Quiescent SAA, Parkinson's disease, Seeding activity

Introduction

Synucleinopathies, a group of neurodegenerative disorders including Parkinson's disease (PD), dementia with Lewy bodies (DLB), and multiple system atrophy (MSA), are characterized by the pathological aggregation of the protein α-synuclein (αSyn)[1,2]. In these diseases, αSyn transitions from its soluble, functional form into misfolded, self-replicating aggregates[3,4]. This aberrant αSyn, capable of recruiting and converting native αSyn into its pathological form, propagates throughout the nervous system in a prion-like manner, acting as a "seed" that amplifies the disease process[5,6]. The seeding activity, characterized by the ability of aggregated αSyn to induce further aggregation in neighboring cells after being taken up through endocytosis or released via exocytosis, is central to disease progression[7,8]. These misfolded αSyn aggregates can coalesce into larger, insoluble structures, such as the Lewy bodies (LBs) that are hallmark features of these diseases and contribute to neuronal dysfunction and death[9]. Therefore, understanding the spatial distribution, propagation, and particularly the seeding activity of these aggregates is crucial for elucidating the underlying mechanisms of synucleinopathies and developing effective therapeutic interventions.

While traditional antibody-based approaches have been instrumental in identifying and localizing pathological αSyn aggregates, often relying on markers like phosphorylation at Serine 129 (pS129) that are elevated in diseased brains[10], they are inherently limited in their ability to capture the dynamic seeding activity that defines the pathological process. These methods primarily provide a static snapshot of aggregate load or post-translational modifications[11], but they do not directly measure the functional capacity of aggregates to initiate and propagate the disease.

To address this critical gap, seed amplification assays (SAAs) have emerged as powerful tools[12,13]. SAAs leverage the inherent seeding activity of misfolded proteins by providing an environment with exogenous monomeric substrates that allow for the amplification of even minute quantities of pathological seeds in vitro[14,15]. However, conventional SAAs rely on agitation, such as shaking or sonication, to enhance amplification efficiency by fragmenting growing fibrils and increasing the number of available seeding ends[16,17]. While effective for amplification, this mechanical disruption obliterates spatial information, making it impossible to ascertain the original location of seeds within the tissue context.

To overcome these limitations and measure the seeding activity with spatial resolution, we developed the αSyn Quiescent Seed Amplification Assay (αSyn QSAA), a novel technique designed for in situ amplification of αSyn seeds within tissue sections. This was achieved by optimizing SAA buffer conditions, including introducing sulfate ions (SO_4^{2-}), elevating the reaction temperature to 70°C, and employing mouse-derived αSyn as a substrate, ultimately achieving seed-dependent elongation under quiescent conditions. We further combined QSAA with immunofluorescence (IF), creating IF-QSAA, to allow for simultaneous visualization of amplified seeds and specific target proteins through antibody labeling. This technique is also adaptable for use with a variety of anti-αSyn antibodies, facilitating the investigation of complex relationships between αSyn phosphorylation, aggregation, and seeding activity. The development of QSAA and IF-QSAA provides a new approach for investigating the intricacies of αSyn seeding and propagation, offering critical insights into the pathogenesis of synucleinopathies and holding significant promise for advancing diagnostic and therapeutic strategies.

Results

Development of a quiescent system for αSyn seed amplification

A quiescent incubation environment is essential for *in situ* seed amplification, but

transitioning from a shaking-based to a quiescent system necessitates sustained amplification efficiency. Traditional SAAs rely on intermittent cycles of shaking or sonication[18,19], interspersed with periods of quiescent elongation (**Figure 1a**). These agitation cycles fragment growing fibrils, generating new active ends and resetting seed amplification, thus promoting rapid and sustained fibril growth[16,17]. Without fragmentation, fibril elongation eventually plateaus, slowing the amplification rate. Therefore, achieving efficient quiescent amplification requires a robust, fragmentation-independent mechanism that sustains fibril growth.

To this end, we explored strategies to enhance fibril elongation without mechanical disruption. As schematically illustrated in **Figure 1b**, it compares the mechanisms of intermittent shaking (upper panel) and our proposed quiescent amplification strategy (lower panel). Building on previous studies demonstrating that substrate modifications[12], specific additives[20-23], and elevated temperatures[24,25] can accelerate fibril growth, we systematically tested the effects of: 1) replacing wild-type human αSyn monomer (HM) with mouse αSyn monomer (MM), which contains a natural mutation analogous to human A53T (**Figure 1c**); 2) incorporating sulfate ions (SO_4^{2-}, Na_2SO_4) into the reaction buffer; and 3) increasing the incubation temperature to 70°C. While each modification on its own significantly accelerated the onset of αSyn PFFs amplification in the presence of shaking (**Figure 1d-e**), this effect was not mirrored under quiescent conditions.

We then combined these modifications to assess their synergistic effects under both shaking (cyclic fragmentation) and quiescent conditions. Using 1pg PFFs seeding, the combination of MM, SO_4^{2-}, and 70°C dramatically accelerated amplification in the shaking system (**Figure 1f**), but it also resulted in significant spontaneous fibril formation, as indicated by the low folding separation (FS, PAR_{1pg}/PAR_{ns} = 1.102). Remarkably, under quiescent conditions, the same combination (MM, +SO_4^{2-}, 70°C) enabled rapid and highly

specific amplification of the αSyn seeds (lag phase ≈ 13 h), with no detectable spontaneous fibrillation within 100 hours (**Figure 1g**).

Transmission electron microscopy (TEM) analysis confirmed the fibrillar morphology of the amplification products, with two distinct morphologies observed: densely packed fibrillar aggregates and loosely associated fibrillar assemblies (**Figure 1h**). These results demonstrate that the optimized quiescent system (MM, $+SO_4^{2-}$, 70°C) allowed amplifying αSyn seeds without the need for mechanical agitation, and built up a new amplification method called QSAA.

QSAA enables *in situ* amplification of pathological αSyn seeds in tissue sections

Building upon our previous success in quiescently amplifying αSyn aggregates in a liquid system, we investigated whether QSAA could be adapted in situ within tissue sections. To this end, we validated this method using a well-established mouse model of LB pathology induced by intrastriatal injection of mouse αSyn preformed fibrils (mPFFs)[26,27]. A workflow (**Figure 2a, Supplementary Figure 1**) was applied to coronal, sagittal, and horizontal brain sections from mPFFs-injected mice 90 days post-injection (dpi). After a five-hour incubation, robust ThT fluorescence was observed throughout the brains, indicating widespread αSyn seeding activity. The signal was most intense at the injection site within the striatum (STR), exhibiting a gradient-like decrease in intensity with increasing distance from the injection core (**Figure 2b,** coronal). Beyond the injection site, αSyn seeding activity was widely distributed in regions interconnected with the STR, including the bilateral corpus callosum (CC), anterior commissure (AC), the walls of the lateral ventricles, and cortical areas such as the primary and secondary motor cortex (M1, M2), secondary somatosensory cortex (S2), and ectorhinal cortex (ECT) (**Figure 2b,** coronal). This distribution was consistent across sagittal and horizontal sections (**Figure 2b**, sagittal and horizontal), with sagittal sections notably showing the spread of seeding activity along the anterior commissure, olfactory limb

(ACO) towards the olfactory bulb (OB).

Furthermore, we generated the first whole-brain mapping of αSyn seeding activity in mPFFs-injected mouse brains across coronal, sagittal, and horizontal sections (**Supplementary Figure 2, 3, 4**). To compare the distribution of QSAA-amplified seeding activity with pathological αSyn, we performed immunofluorescence (IF) staining for pS129-αSyn, a widely used marker for LB pathology, on consecutive brain sections (**Supplementary Figure 2**). QSAA and pS129-αSyn staining exhibited largely overlapping distributions, with prominent bilateral signals in the STR, M1, M2, S2, ECT, and amygdala (AMY). Both techniques also revealed unilateral labeling (ipsilateral to the injection) in the insular cortex (IC), piriform cortex (PIR), olfactory tubercle (OT), claustrum (CLA), dorsal endopiriform nucleus (DEn), intermediate endopiriform nucleus (IEn), substantia nigra pars reticulata (SNr), substantia nigra pars compacta (SNc), ventral tegmental area (VTA), and parabrachial pigmented nucleus of the VTA (PBP), with some signal also detected in the brainstem. Notably, neither pS129-αSyn immunoreactivity nor QSAA signal was observed in the bilateral hippocampus (HIP), contralateral thalamus (TH), contralateral SN, or cerebellum (CB). Importantly, despite the overall concordance, QSAA signals were more extensively distributed as compared to pS129-αSyn immunofluorescence, particularly within fiber tracts such as the bilateral CC, anterior commissure, anterior part (ACA) and anterior commissure, posterior part (ACP), and the ipsilateral internal capsule (IC), external capsule (EC), medial forebrain bundle (MFB), fasciculus retroflexus (FR), and nigrostriatal tract (NST). This suggests that QSAA is well-suited to detect αSyn seeds within white matter tracts, where pS129-αSyn detection is limited may result from the paucity of neuronal somata and the correspondingly low physiological levels of αSyn.

Further investigation of the *in situ* amplification products using TEM revealed two distinct morphologies: compact aggregates confined within the interstitial space of the tissue, often

displaying concentric ring-like arrangements and incorporating cellular debris (**Figure 2c**, upper panel), and loosely arranged, radiating aggregates on the tissue surface (**Figure 2c**, lower panel). Additionally, droplet-like aggregates of varying sizes were observed clustered around the nucleus (**Figure 2d**). These TEM observations confirm the fibrillar nature of the QSAA product and demonstrate its utility in visualizing and localizing αSyn seeding activity at the cellular level.

To assess the capability of QSAA to detect endogenous αSyn seeding activity *in situ*, we analyzed postmortem brain tissue from individuals with PD (n=4), progressive supranuclear palsy (PSP, n=3), and healthy controls (HC, n=3). QSAA successfully amplified αSyn seeds in PD brain sections, producing robust ThT fluorescence, while no signal was detected in PSP or HC brains (**Figure 2e**). IF staining for pS129-αSyn also confirmed the presence of pathological aggregates exclusively in PD samples, mirroring the QSAA results (**Figure 2e**). To gain insight into the dynamics of this *in situ* amplification, we performed a dynamic observation of QSAA on PD brain sections (**Supplementary Video**). Faint ThT signals emerged as early as 1 hour, with increased fluorescence over time.

IF-QSAA: a dual-fluorescence approach to visualize αSyn seeding with antibodies at the cellular level

IF is a technique employed to localize specific proteins by utilizing specific antibodies. We were intrigued by the possibility of integrating QSAA with IF on tissue sections to precisely determine the spatial location of proteins associated with αSyn seeding. The ThT dye used in QSAA has an excitation range of 420–460 nm and an emission range of 470–510 nm. To prevent spectral overlap with ThT, we opted for the far-red Alexa Fluor 647 dye in IF, allowing for dual fluorescence labeling (**Figure 3a**). mPFFs were injected into the SNc and the mice were sacrificed 90 days later. Initially, we performed QSAA prior to IF staining. Unfortunately, performing QSAA prior to IF resulted in a notable loss of antibody epitopes,

as evidenced by the reduced number of NeuN signals in brain sections compared to those subjected to NeuN single staining (**Figure 3b**). In contrast, when IF staining was performed before QSAA treatment, clear signals for both NeuN and ThT were observed, similar to those obtained with single staining, suggesting that QSAA does not interfere with IF staining. Based on these results, we adopted a protocol where IF staining precedes QSAA treatment for dual fluorescence staining.

Using IF-QSAA, we analyzed the coexistence of αSyn seeds (labeled green) with NeuN or GFAP in the aforementioned samples (**Figure 3c**). Our results showed that the injection site (SNc) exhibited the highest concentration of green fluorescence signals, indicating the seeding activity of αSyn seeds. Additionally, we observed a statistically significant decrease in NeuN-positive neurons and an increase in GFAP-positive astrocytes at the injection site. These findings align with previous research demonstrating that αSyn seeds induce neurotoxicity and reactive astrogliosis.

To further explore the relationship between αSyn aggregates and QSAA products, we labeled aggregated αSyn using a mouse-specific αSyn antibody (D37A6) and examined its localization with amplification products (**Figure 3d**). Dual staining revealed a strong correlation between the ThT signal and αSyn aggregates at the injection site. Specifically, the mixed signal exhibited a "halo-like" pattern, with antibody-labeled aggregates at the core surrounded by a gradually fading halo of the ThT signal (**Figure 3d**, arrows). This correlation strongly suggested that the seeding activity detected by QSAA was closely linked to pre-existing αSyn aggregation, confirming that the ThT signals from quiescent amplification originated from these aggregated αSyn seeds. To further clarify the composition of QSAA products, we first performed QSAA in the aforementioned sections and then stained the QSAA products using the mouse-specific αSyn antibody (D37A6) (**Figure 3e**). The results showed that ThT signals, which indicate newly formed beta-sheet structures, were surrounded

by a layer of red signals (**Figure 3e**, arrowheads). This confirmed that αSyn seeds recruit and convert exogenous monomers through QSAA (**Figure 3f**).

To gain a deeper understanding of QSAA product localization, we employed high-resolution confocal microscopy on sections processed with IF-QSAA. Brain sections from mice injected with mPFFs into the striatum and euthanized 90 days post-injection were subjected to NeuN staining followed by QSAA. Confocal microscopy revealed that QSAA staining produced dense, oval-shaped structures located within the soma of NeuN-positive neurons. Some ThT signals were confined within neurons (**Figure 3g**, arrows), while others formed large aggregates, exceeding 50 μm in diameter and extending beyond the cellular boundaries (**Figure 3g**, arrowheads). In contrast, control mice injected with MM only showed NeuN signals. These findings demonstrate that IF-QSAA effectively elucidates the intricate spatial relationships between different cell types and αSyn seeding, providing deeper insights into αSyn seeding at the cellular level.

IF-QSAA reveals distinct distributions of αSyn aggregates and seeding activity

After determining that QSAA can be effectively used in combination with IF, we conducted dual-labeling experiments using the IF-QSAA technique to examine whether the seeding activity of pathological αSyn aligns with the aggregates represented by antibodies. Three different αSyn antibodies were analyzed: pS129 (EP1536Y) **(Figure 4a**), total αSyn (2642) (**Figure 4b**), and mouse αSyn (D37A6) (**Figure 4c**). Initially, mPFFs were injected into the cortex, hippocampus, and substantia nigra of mice. Six months post-injection, this model exhibited enhanced propagation of pathological αSyn throughout the brain. Our analysis focused on two regions, the CC and the MFB, which are rich in projection fibers crucial for transmission. These regions exhibited notable differences between QSAA signals and antibody-detected aggregates (**Supplementary Figure 2**), suggesting potential discrepancies between αSyn seeding and protein aggregation.

After three hours of incubation, we observed that both QSAA and antibody signals were significantly stronger in the CC compared to the MFB (**Figure 4d-g**). Moreover, in most cases, antibody and QSAA signals together formed a characteristic " halo-like" pattern, where antibody-positive aggregates formed a core region surrounded by QSAA amplification products. Interestingly, not all QSAA amplification products were associated with antibody-positive cores and not all antibody-positive aggregates were surrounded by QSAA products. To quantify these differences, we calculated the percentage of antibody signals co-localizing with QSAA products, representing the prevalence of the " halo-like" pattern among all QSAA-positive signals. The pS129 antibody showed a significantly higher co-localization percentage with QSAA products compared to the other two antibodies (**Figure 4h**). This suggests a stronger association between phosphorylated αSyn and seeding activity. As illustrated in **Figure 4i**, the pathological state of αSyn can be categorized into four combinations based on IF-QSAA: pS129+/QSAA+, pS129+/QSAA-, pS129-/QSAA+, and pS129-/QSAA-. The difference between pS129 and αSyn seeding observed in the same samples suggests that molecular modifications such as pS129 may occur following the initial aggregation of αSyn. This highlights the complementary nature of QSAA and antibody-based approaches. Overall, by leveraging QSAA alongside traditional immunodetection techniques, IF-QSAA may provide a more nuanced and comprehensive assessment of αSyn seeding and aggregation, offering critical insights into the dynamics of αSyn seeding pathology.

Discussion

αSyn seeding activity, a hallmark of its misfolded form, drives its prion-like propagation and plays a central role in the pathology of LB-related diseases[26]. However, existing methods for detecting αSyn seeding activity are significantly limited. Antibody-based techniques primarily identify pre-formed aggregates[28] and cannot directly assess seeding activity. While traditional SAAs can detect seeding activity, they require tissue homogenization and rely on

vigorous shaking or ultrasonication[29,30], which disrupts the spatial localization of seeds, making it impossible to determine their distribution in specific regions. To address this challenge, we developed a QSAA designed to amplify αSyn seeds in situ while preserving their spatial localization. Unlike standard SAAs that rely on cyclic fibril fragmentation, QSAA leverages the intrinsic seeding properties of αSyn through a fundamentally different approach[31-33]. This method employs a quiescent amplification system enhanced by sulfate ions (SO_4^{2-}), which promote electrostatic interactions to fibril elongation and stabilize misfolded protein aggregates[20,21]. By combining these conditions with an elevated reaction temperature of 70°C[24,25] and a mouse-derived αSyn substrate[34,35], QSAA robustly amplifies αSyn seeds while effectively suppressing spontaneous nucleation.

QSAA and antibody-based detection methods have both similarities and differences when analyzing pathological αSyn. Both techniques enable the localization of pathological αSyn in tissue sections, providing insights into the spatiotemporal dynamics of αSyn pathology in biopsy and autopsy samples from PD patients[36,37]. However, conventional immunological techniques for detecting αSyn deposition have yielded inconsistent results. For example, some studies have concluded that IHC is unsuitable for PD diagnosis[38], while others report a detection rate of over 90% for pathological αSyn in skin samples from PD patient cohorts[37]. These discrepancies are likely attributable to the limited sensitivity of antibody-based methods[39]. In contrast, QSAA demonstrates significantly superior sensitivity, capable of detecting as little as 1 pg of αSyn seeds. This heightened sensitivity is coupled with high specificity, evidenced by a fold separation (FS) exceeding 7. Despite these advantages, QSAA currently cannot differentiate between distinct αSyn strains[7,40,41] or identify various post-translational modifications (PTMs) [42,43]. Future research could focus on analyzing fluorescence properties or conformational differences of the amplification products to overcome these limitations and expand QSAA's applications in strain variation studies[41].

Compared to traditional SAAs, QSAA provides the unique advantage of in situ seeding activity assessment while enabling rapid detection of αSyn seeding within just 5 hours in brain samples from mPFFs-injected mice and PD patients, achieving high diagnostic accuracy and specificity. Conversely, the amplification phase for SAA under standard buffer conditions typically takes more than 12 hours[12,18], significantly longer than QSAA. However, QSAA's application to biological fluids, such as serum, remains limited. This limitation may arise from the complex components in biological samples that interfere with reaction efficiency[44,45]. Future efforts should aim to develop more robust amplification systems or optimize sample pre-treatment protocols to expand the utility of QSAA for body fluid diagnostics[44-46].

QSAA experiments must carefully address the risk of false positives or spontaneous aggregation. While removing the "quaking" factor can help reduce spontaneous aggregation of αSyn monomers, QSAA still faces challenges that could lead to false positives. For example, during tissue sectioning, seed fragments may detach and contaminate areas devoid of seeds, while fluid convection during incubation could subtly shift the position of amplified products. Fortunately, our experimental results demonstrate that QSAA signals show distinct, brain region-specific distribution patterns, which align with the pathology of PFFs-induced LB propagation[27,47], confirming the reliability of these findings. Additionally, optimizing experimental protocols—such as limiting incubation times and standardizing sectioning techniques—can further reduce the occurrence of false positives.

QSAA offers a powerful method for *in situ* amplification of misfolded proteins by leveraging their intrinsic self-replication properties. This allows for precise spatial localization of protein seeds with high sensitivity and specificity. This breakthrough presents new opportunities to study αSyn aggregates in diseases related to Lewy bodies. By refining additive formulations and utilizing various protein substrates, QSAA can potentially be adapted to other misfolded

proteins, such as Tau and TDP-43, particularly those that have already demonstrated the ability to undergo cyclic fragmentation amplification in in vitro SAA experiments[48,49]. These capabilities make QSAA an essential tool for exploring disease mechanisms, identifying biomarkers, and advancing therapeutic development, particularly in evaluating therapies aimed at targeting protein aggregation and propagation.

Methods

Generation of αSyn monomers and PFFs

Full-length mouse αSyn (1–140 amino acids) was purified with minor modifications to a previously established protocol[50]. Briefly, *E. coli* BL21 (DE3) cells (TransGen) were transformed with a plasmid encoding full-length mouse *Snca*. Cultures were grown overnight at 230 rpm to an OD600 of 0.8 and induced with 1.0 mM isopropyl β-D-thiogalactoside for 4 hours. Cells were harvested by centrifugation (8000 x g, 10 min, 4°C) and lysed by sonication in high-salt buffer (10 mM Tris-HCl [pH 7.5], 500 mM NaCl, 1 mM EDTA, 1 mM PMSF, and protease inhibitors). The lysate was boiled for 10 min and centrifuged (20,000 x g, 30 min, 4°C). αSyn was precipitated with 45% saturated ammonium sulfate, resuspended in 10 mM Tris-HCl (pH 7.5) with 50 mM NaCl, and acidified to pH 3.0 with HCl. Precipitated proteins were removed by centrifugation, and the supernatant pH was adjusted to 7.5 with NaOH. αSyn was further purified using a HiTrap column (GE Healthcare), dialyzed against 10 mM Tris-HCl (pH 7.5) with 50 mM NaCl, and filtered through a 100-kDa Amicon Ultra filter (Millipore).

To generate PFFs, purified αSyn monomer was diluted in 10 mM Tris-HCl (pH 7.5) with 50 mM NaCl and shaken at 1000 rpm for 5–7 days (Eppendorf). PFFs were then sonicated at 20% power for 60 pulses (1-s on/1-s off).

SAA and ThT assay

To assess αSyn aggregation kinetics under agitation, PFFs or PBS were added to 1 mg/ml mouse αSyn monomers with 50 mM NaCl, 10 mM Tris-HCl (pH 7.5), and 40 μM ThT in amplification buffer (total volume: 100 μl). Samples included 800 mM sodium sulfate as a seeding enhancer or no additive. Each mixture was transferred to a 96-well plate, sealed (BioTss, Beijing, China), and loaded into a SpectraMax iD5 plate reader (Molecular Device, San Jose, CA) for incubation at 37°C with cyclic agitation (1 min agitation, 14 min rest). ThT fluorescence (excitation: 450 nm, emission: 490 nm) was monitored over time.

To assess αSyn aggregation kinetics under quiescent conditions, PFFs or PBS were added to 1 mg/ml mouse αSyn monomers with 25 mM NaCl, 800 mM sodium sulfate, and 40 μM ThT in amplification buffer at the pH 6.0 (total volume: 20 μl). Each mixture was transferred to a 96-well polypropylene PCR plate and overlaid with 20 μl of paraffin oil to prevent evaporation. The plate was sealed (BioTss, Beijing, China) and loaded into a real-time PCR instrument for incubation at 37°C or 70°C without agitation. ThT fluorescence intensity was monitored over time using the FAM channel (excitation: 452–486 nm, emission: 505–545 nm).

For both assays, the lag time was determined from the resulting aggregation curves as the time required to reach threshold fluorescence (background fluorescence plus 5 standard deviations). The protein aggregation rate was calculated as 1/lag phase.

Animals and stereotaxic injections

All animal procedures were performed in accordance with ethical regulations and approved by the Institutional Animal Care and Use Committee of Guangzhou Medical University. Male C57BL/6 mice (10–12 weeks old) were housed under standard conditions with a 12-hour light/dark cycle and ad libitum access to food and water. Mice received unilateral stereotaxic injections of mPFFs (5 mg/ml) or MM under isoflurane anesthesia. Three injection paradigms were employed: 1) striatum: 1 μl into the right striatum (ML, −2.0 mm;

AP, 0.8 mm; DV, −3.5 mm); 2) substantia nigra: 1 μl into the right substantia nigra (ML, −1.0 mm; AP, 3.08 mm; DV, −4.5 mm); and 3) cortical, hippocampal, and substantia nigra: 1 μl into the right cortex (ML, 0.0 mm; AP, 1.5 mm; DV, −1.6 mm), hippocampus (ML, −1.7 mm; AP, 2.5 mm; DV, −1.8 mm), and substantia nigra (ML, −1.0 mm; AP, 3.08 mm; DV, −4.5 mm). Injections were performed at 1 μl/min using a stereotactic alignment system (Kopf Instruments). The Hamilton syringe remained in place for 5 minutes post-injection. Researchers were blinded to experimental conditions. At 1–6 months post-injection, mice were transcranial perfused with ice-cold 4%PFA under isoflurane anesthesia. Brains were collected for sectioning and *in situ* amplification of αSyn aggregates.

Brain Specimens

Ten autopsy brain samples were obtained from the First Affiliated Hospital of Guangzhou Medical University between 2005 and 2022, including 4 from PD patients, 3 from PSP patients, and 3 from healthy controls. Brains were collected within 12 hours of death and sagittally sectioned. The left hemisphere was fixed in 10% buffered formaldehyde, while the right hemisphere was coronally sectioned and frozen at -80 ℃. The sample collection methodology was approved by the Ethics Committee of the First Affiliated Hospital of Guangzhou Medical University (MRE. No.155).

αSyn QSAA and IF-QSAA

Sample preparation: Fresh brain tissues were fixed in 4% paraformaldehyde (PFA) for 24 h, followed by dehydration in 30% sucrose solution for 48 h. Tissues were embedded in the OCT compound, and 14-μm-thick sections were cut and subjected to secondary fixation using acetone at -20°C for 10 min and air-dried.

Immunofluorescence (Optional): Sections were permeabilized with 0.5% Triton X-100 for 10 min. Nonspecific binding sites were blocked with 5% BSA for 10 min. Sections were incubated with primary antibodies, including anti-phosphorylated αSyn EP1536Y (CST, No.

51253, 1:500), anti-total αSyn (CST, No.2642S, 1:500), and anti-Mouse αSyn D37A6 (CST, No. 4179S, 1:500) at room temperature (RT) for 4 h. Sections were then incubated with Alexa Fluor 647-labeled (1:1000) secondary antibody at RT for 1 h.

QSAA: Sections were placed in a humid chamber and incubated with 200 µl QSAA buffer containing 1 mg/ml MM, 800 mM sodium sulfate, 40 µM ThT, 25 mM NaCl, 10 mM Tris-HCl, at pH 6.0 at 70°C for 0-6 h. Fluorescence images were collected in the FITC channel through a fluorescence microscope (NIKON ECLIPSE 3000, Tokyo, Japan) after 3 gentle washes in PBS (1 min/wash). To obtain high-resolution fluorescent microscopic images of the amplified products in brain tissues, the slides were placed on a motorized stage, and images were captured at 20× and 63× magnifications using an SP8 Leica scanning confocal microscope. Specifically, a 50 µm-thick z-stack with a 2-µm step size in the FITC channel was acquired to visualize the QSAA amplification products.

Transmission electron microscopy

For amplification products of PFFs: A 10 µl volume of amplification products were loaded onto freshly glow-discharged 400 mesh carbon-coated copper grids (Zhongjingkeyi Technology, Beijing, China) for 2 minutes. The grid was rinsed with 50 mM Tris-HCL (pH 7.5) and then floated on 0.75% uranium formate (Solarbio, Beijing, China). The grids were observed using a CM 120 transmission electron microscope (PHILIPS, Eindhoven, The Netherlands) at an acceleration voltage of 80-120 kV.

For *in situ* amplified products: Amplified brain tissues were harvested, immediately fixed in TEM fixative at 4°C, and washed with 0.1 M phosphate buffer (PB, pH 7.4). Tissues were post-fixed with 1% osmium tetroxide in 0.1 M PB (pH 7.4) for 2 hours at room temperature, followed by rinsing in 0.1 M PB (pH 7.4). Dehydration was performed at room temperature using a graded ethanol series (30%, 50%, 70%, 80%, 95%, and 100%) and acetone. The samples were then infiltrated with a mixture of acetone and EMBed 812 resin at 37°C,

followed by embedding in pure EMBed 812 resin. Polymerization was carried out in a 60°C oven for more than 48 hours. The resin blocks were sectioned into 1.5 μm slices using a semi-thin microtome, stained with toluidine blue, and positioned under a light microscope. Ultrathin sections (60-80 nm) were cut using an ultramicrotome and placed onto 150 mesh copper grids with formvar film. Staining was performed using 2% uranyl acetate saturated alcohol solution and 2.6% lead citrate, avoiding CO2 exposure. After drying, the grids were observed under a TEM, and images were captured.

Statistical analysis

All statistical analyses were conducted with the GraphPad Prism software (San Diego, CA). Experimental data were analyzed using the two-tailed independent Student's *t*-test for comparing two groups and one-way analysis of variance (ANOVA) followed by Tukey's post-hoc test for comparison among three or more groups. Unless otherwise stated, data are presented as mean ± SD. $P < 0.05$ was considered statistically significant.

Data availability

This paper does not report the original code. Any additional information required to reanalyze the data reported in this report is available from the lead contact upon request. All materials used in this study will be made available subject to a materials transfer agreement.

Acknowledgments

This work was supported by grants from the National Natural Science Foundation of China (grant numbers 81870856, 81870992, and 32171236).

Author contributions

H.M. designed the study, performed experiments, and wrote the manuscript. Y.K. supervised experiments, analyzed data, and contributed to manuscript preparation. D.W. and H.L. assisted with experimental procedures and data collection. P-Y.X. provided project oversight, funding, and critical revisions to the manuscript.

Competing interests

The authors declare that they have no competing interests.

Reference

1 Schweighauser, M. *et al.* Structures of α-synuclein filaments from multiple system atrophy. *Nature* **585**, 464-469 (2020). https://doi.org/10.1038/s41586-020-2317-6

2 Yang, Y. *et al.* Structures of α-synuclein filaments from human brains with Lewy pathology. *Nature* **610**, 791-795 (2022). https://doi.org/10.1038/s41586-022-05319-3

3 Rodriguez, J. A. *et al.* Structure of the toxic core of α-synuclein from invisible crystals. *Nature* **525**, 486-490 (2015). https://doi.org/10.1038/nature15368

4 Theillet, F. X. *et al.* Structural disorder of monomeric α-synuclein persists in mammalian cells. *Nature* **530**, 45-50 (2016). https://doi.org/10.1038/nature16531

5 Luk, K. C. *et al.* Intracerebral inoculation of pathological α-synuclein initiates a rapidly progressive neurodegenerative α-synucleinopathy in mice. *J Exp Med* **209**, 975-986 (2012). https://doi.org/10.1084/jem.20112457

6 Luk, K. C. *et al.* Exogenous alpha-synuclein fibrils seed the formation of Lewy body-like intracellular inclusions in cultured cells. *Proc Natl Acad Sci U S A* **106**, 20051-20056 (2009). https://doi.org/10.1073/pnas.0908005106

7 Peng, C. *et al.* Cellular milieu imparts distinct pathological α-synuclein strains in α-synucleinopathies. *Nature* **557**, 558-563 (2018). https://doi.org/10.1038/s41586-018-0104-4

8 Hansen, C. *et al.* α-Synuclein propagates from mouse brain to grafted dopaminergic neurons and seeds aggregation in cultured human cells. *J Clin Invest* **121**, 715-725 (2011). https://doi.org/10.1172/jci43366

9 Volpicelli-Daley, L. A. *et al.* Exogenous α-synuclein fibrils induce Lewy body pathology leading to synaptic dysfunction and neuron death. *Neuron* **72**, 57-71 (2011). https://doi.org/10.1016/j.neuron.2011.08.033

10 Anderson, J. P. *et al.* Phosphorylation of Ser-129 is the dominant pathological modification of alpha-synuclein in familial and sporadic Lewy body disease. *J Biol Chem* **281**, 29739-29752 (2006). https://doi.org/10.1074/jbc.M600933200

11 Mahul-Mellier, A. L. *et al.* The process of Lewy body formation, rather than simply α-synuclein fibrillization, is one of the major drivers of neurodegeneration. *Proc Natl Acad Sci U S A* **117**, 4971-4982 (2020). https://doi.org/10.1073/pnas.1913904117

12 Groveman, B. R. *et al.* Rapid and ultra-sensitive quantitation of disease-associated α-synuclein seeds in brain and cerebrospinal fluid by αSyn RT-QuIC. *Acta Neuropathol Commun* **6**, 7 (2018). https://doi.org/10.1186/s40478-018-0508-2

13 Shahnawaz, M. *et al.* Development of a Biochemical Diagnosis of Parkinson Disease by Detection of α-Synuclein Misfolded Aggregates in Cerebrospinal Fluid. *JAMA Neurol* **74**, 163-172 (2017). https://doi.org/10.1001/jamaneurol.2016.4547

14 Saborio, G. P., Permanne, B. & Soto, C. Sensitive detection of pathological prion protein by cyclic amplification of protein misfolding. *Nature* **411**, 810-813 (2001). https://doi.org/10.1038/35081095

15 Atarashi, R. *et al.* Ultrasensitive human prion detection in cerebrospinal fluid by real-time quaking-induced conversion. *Nat Med* **17**, 175-178 (2011). https://doi.org/10.1038/nm.2294

16 Soto, C., Saborio, G. P. & Anderes, L. Cyclic amplification of protein misfolding: application to prion-

related disorders and beyond. *Trends Neurosci* **25**, 390-394 (2002). https://doi.org/10.1016/s0166-2236(02)02195-1

17 Paciotti, S., Bellomo, G., Gatticchi, L. & Parnetti, L. Are We Ready for Detecting α-Synuclein Prone to Aggregation in Patients? The Case of "Protein-Misfolding Cyclic Amplification" and "Real-Time Quaking-Induced Conversion" as Diagnostic Tools. *Front Neurol* **9**, 415 (2018). https://doi.org/10.3389/fneur.2018.00415

18 Concha-Marambio, L., Pritzkow, S., Shahnawaz, M., Farris, C. M. & Soto, C. Seed amplification assay for the detection of pathologic alpha-synuclein aggregates in cerebrospinal fluid. *Nat Protoc* **18**, 1179-1196 (2023). https://doi.org/10.1038/s41596-022-00787-3

19 Rossi, M. *et al.* Ultrasensitive RT-QuIC assay with high sensitivity and specificity for Lewy body-associated synucleinopathies. *Acta Neuropathol* **140**, 49-62 (2020). https://doi.org/10.1007/s00401-020-02160-8

20 Munishkina, L. A., Henriques, J., Uversky, V. N. & Fink, A. L. Role of protein-water interactions and electrostatics in alpha-synuclein fibril formation. *Biochemistry* **43**, 3289-3300 (2004). https://doi.org/10.1021/bi034938r

21 Metrick, M. A., 2nd *et al.* Million-fold sensitivity enhancement in proteopathic seed amplification assays for biospecimens by Hofmeister ion comparisons. *Proc Natl Acad Sci U S A* **116**, 23029-23039 (2019). https://doi.org/10.1073/pnas.1909322116

22 Giehm, L., Oliveira, C. L., Christiansen, G., Pedersen, J. S. & Otzen, D. E. SDS-induced fibrillation of alpha-synuclein: an alternative fibrillation pathway. *J Mol Biol* **401**, 115-133 (2010). https://doi.org/10.1016/j.jmb.2010.05.060

23 Giehm, L. & Otzen, D. E. Strategies to increase the reproducibility of protein fibrillization in plate reader assays. *Anal Biochem* **400**, 270-281 (2010). https://doi.org/10.1016/j.ab.2010.02.001

24 Orrú, C. D. *et al.* Rapid and sensitive RT-QuIC detection of human Creutzfeldt-Jakob disease using cerebrospinal fluid. *mBio* **6** (2015). https://doi.org/10.1128/mBio.02451-14

25 Bhumkar, A. *et al.* Single-Molecule Counting Coupled to Rapid Amplification Enables Detection of alpha-Synuclein Aggregates in Cerebrospinal Fluid of Parkinson's Disease Patients. *Angew Chem Int Ed Engl* **60**, 11874-11883 (2021). https://doi.org/10.1002/anie.202014898

26 Uemura, N. *et al.* α-Synuclein aggregates amplified from patient-derived Lewy bodies recapitulate Lewy body diseases in mice. *Nat Commun* **14**, 6892 (2023). https://doi.org/10.1038/s41467-023-42705-5

27 Luk, K. C. *et al.* Pathological α-synuclein transmission initiates Parkinson-like neurodegeneration in nontransgenic mice. *Science* **338**, 949-953 (2012). https://doi.org/10.1126/science.1227157

28 Kumar, S. T. *et al.* How specific are the conformation-specific α-synuclein antibodies? Characterization and validation of 16 α-synuclein conformation-specific antibodies using well-characterized preparations of α-synuclein monomers, fibrils and oligomers with distinct structures and morphology. *Neurobiol Dis* **146**, 105086 (2020). https://doi.org/10.1016/j.nbd.2020.105086

29 Soto, C. α-Synuclein seed amplification technology for Parkinson's disease and related synucleinopathies. *Trends Biotechnol* **42**, 829-841 (2024). https://doi.org/10.1016/j.tibtech.2024.01.007

30 Vascellari, S., Orrù, C. D. & Caughey, B. Real-Time Quaking- Induced Conversion Assays for Prion Diseases, Synucleinopathies, and Tauopathies. *Front Aging Neurosci* **14**, 853050 (2022). https://doi.org/10.3389/fnagi.2022.853050

31 Bhumkar, A. *et al.* Single-Molecule Counting Coupled to Rapid Amplification Enables Detection of α-Synuclein Aggregates in Cerebrospinal Fluid of Parkinson's Disease Patients. *Angew Chem Int Ed Engl*

60, 11874-11883 (2021). https://doi.org/10.1002/anie.202014898

32 Horne, R. I. *et al.* Secondary Processes Dominate the Quiescent, Spontaneous Aggregation of α-Synuclein at Physiological pH with Sodium Salts. *ACS Chem Neurosci* **14**, 3125-3131 (2023). https://doi.org/10.1021/acschemneuro.3c00282

33 Buell, A. K. *et al.* Solution conditions determine the relative importance of nucleation and growth processes in α-synuclein aggregation. *Proc Natl Acad Sci U S A* **111**, 7671-7676 (2014). https://doi.org/10.1073/pnas.1315346111

34 Mao, H. *et al.* Ultrasensitive detection of aggregated α-synuclein using quiescent seed amplification assay for the diagnosis of Parkinson's disease. *Translational Neurodegeneration* **13** (2024). https://doi.org/10.1186/s40035-024-00426-9

35 Kuang, Y. *et al.* α-Synuclein seeding amplification assays for diagnosing synucleinopathies: an innovative tool in clinical implementation. *Translational Neurodegeneration* **13** (2024). https://doi.org/10.1186/s40035-024-00449-2

36 Braak, H. *et al.* Staging of brain pathology related to sporadic Parkinson's disease. *Neurobiol Aging* **24**, 197-211 (2003). https://doi.org/10.1016/s0197-4580(02)00065-9

37 Gibbons, C. H. *et al.* Skin Biopsy Detection of Phosphorylated alpha-Synuclein in Patients With Synucleinopathies. *JAMA* **331**, 1298-1306 (2024). https://doi.org/10.1001/jama.2024.0792

38 Ruffmann, C. *et al.* Detection of alpha-synuclein conformational variants from gastro-intestinal biopsy tissue as a potential biomarker for Parkinson's disease. *Neuropathol Appl Neurobiol* **44**, 722-736 (2018). https://doi.org/10.1111/nan.12486

39 Corbillé, A. G., Neunlist, M. & Derkinderen, P. Cross-linking for the analysis of α-synuclein in the enteric nervous system. *J Neurochem* **139**, 839-847 (2016). https://doi.org/10.1111/jnc.13845

40 Peelaerts, W. *et al.* α-Synuclein strains cause distinct synucleinopathies after local and systemic administration. *Nature* **522**, 340-344 (2015). https://doi.org/10.1038/nature14547

41 Shahnawaz, M. *et al.* Discriminating alpha-synuclein strains in Parkinson's disease and multiple system atrophy. *Nature* **578**, 273-277 (2020). https://doi.org/10.1038/s41586-020-1984-7

42 Zhang, S. *et al.* Post-translational modifications of soluble α-synuclein regulate the amplification of pathological α-synuclein. *Nat Neurosci* **26**, 213-225 (2023). https://doi.org/10.1038/s41593-022-01239-7

43 Altay, M. F., Liu, A. K. L., Holton, J. L., Parkkinen, L. & Lashuel, H. A. Prominent astrocytic alpha-synuclein pathology with unique post-translational modification signatures unveiled across Lewy body disorders. *Acta Neuropathol Commun* **10**, 163 (2022). https://doi.org/10.1186/s40478-022-01468-8

44 Bellomo, G. *et al.* Cerebrospinal fluid lipoproteins inhibit α-synuclein aggregation by interacting with oligomeric species in seed amplification assays. *Mol Neurodegener* **18**, 20 (2023). https://doi.org/10.1186/s13024-023-00613-8

45 Bellomo, G. *et al.* Dissecting the Interactions between Human Serum Albumin and α-Synuclein: New Insights on the Factors Influencing α-Synuclein Aggregation in Biological Fluids. *J Phys Chem B* **123**, 4380-4386 (2019). https://doi.org/10.1021/acs.jpcb.9b02381

46 Davenport, K. A., Hoover, C. E., Denkers, N. D., Mathiason, C. K. & Hoover, E. A. Modified Protein Misfolding Cyclic Amplification Overcomes Real-Time Quaking-Induced Conversion Assay Inhibitors in Deer Saliva To Detect Chronic Wasting Disease Prions. *J Clin Microbiol* **56** (2018). https://doi.org/10.1128/jcm.00947-18

47 Uemura, N. *et al.* alpha-Synuclein aggregates amplified from patient-derived Lewy bodies recapitulate Lewy body diseases in mice. *Nat Commun* **14**, 6892 (2023). https://doi.org/10.1038/s41467-023-

42705-5

48 Scialò, C. *et al.* TDP-43 real-time quaking induced conversion reaction optimization and detection of seeding activity in CSF of amyotrophic lateral sclerosis and frontotemporal dementia patients. *Brain Commun* **2**, fcaa142 (2020). https://doi.org/10.1093/braincomms/fcaa142

49 Kraus, A. *et al.* Seeding selectivity and ultrasensitive detection of tau aggregate conformers of Alzheimer disease. *Acta Neuropathol* **137**, 585-598 (2019). https://doi.org/10.1007/s00401-018-1947-3

50 Volpicelli-Daley, L. A., Luk, K. C. & Lee, V. M. Addition of exogenous α-synuclein preformed fibrils to primary neuronal cultures to seed recruitment of endogenous α-synuclein to Lewy body and Lewy neurite-like aggregates. *Nat Protoc* **9**, 2135-2146 (2014). https://doi.org/10.1038/nprot.2014.143

Figures and figure legend

Figure 1

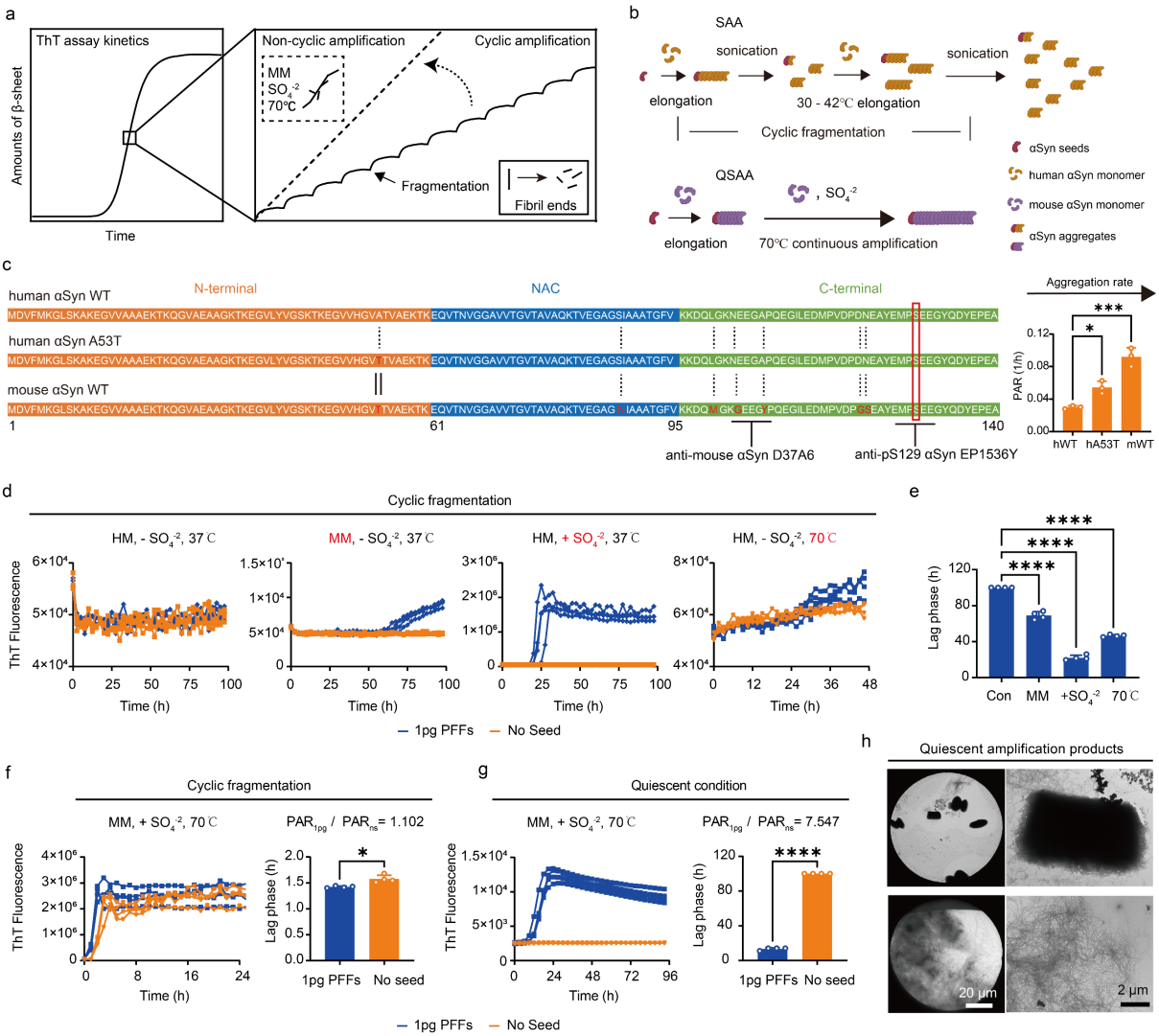

Figure 1. Development of a quiescent system for αSyn seed amplification. a, The left panel presents a schematic diagram depicting the sigmoidal curve characteristic of αSyn aggregation kinetics in ThT assay. The aggregation process was divided into three distinct phases: a lag phase, a growth phase, and a plateau phase. The right panel compares the kinetics of SAA (solid line) with QSAA (dashed line). SAA relies on cyclic fragmentation while QSAA conducted at 70°C with mouse monomers (MM) and SO_4^{2-} (Na_2SO_4), achieves sustained fibril elongation without reaching a plateau, indicating continuous amplification even in the absence of fragmentation. **b,** Mechanistic comparison between SAA and QSAA.

SAA employed intermittent sonication or shaking to fragment fibrils at 30-42°C, generating new ends for monomer addition and elongation. QSAA allowed a continuous amplification at 70°C under quiescent conditions, in the presence of SO_4^{2-} ions. **c,** Sequence alignment of human wild-type (WT) αSyn (hWT), human A53T mutant αSyn (hA53T), and mouse WT αSyn (mWT), amino acid differences are highlighted in red. The aggregation rate increased from hWT to hA53T to mWT. Regions corresponding to the epitopes of anti-mouse αSyn D37A6 and anti-pS129 αSyn EP1536Y antibodies are underlined. **d,** Effects of different conditions on ThT kinetics in a cyclic fragmentation system with seeds (1pg hPFFs, blue) or without seeds (orange). Conditions tested include the presence or absence of SO_4^{2-}, using either human monomer (HM) or mouse monomer (MM) at either 37°C or 70°C. **e,** Comparison of the lag phase from **d**. Data presented as mean ± SD; ****$p < 0.0001$. **f,** Left: Comparison of ThT fluorescence kinetics using MM with SO_4^{2-} at 70°C under cyclic fragmentation conditions, with (blue) or without (orange) 1 pg hPFFs. The lag phase was quantified in the right panel. Folding separation was represented as $PAR_{1pg\ PFFs}/PAR_{no\ seed}$. Data are presented as mean ± SD; *$p < 0.05$. **g,** Left: Comparison of ThT kinetics using MM with SO_4^{2-} at 70°C under quiescent conditions in the presence(blue) or absence(orange) of 1 pg hPFFs. The lag phase was quantified in the right panel. Data are presented as mean ± SD; ****$p < 0.0001$. **h,** TEM analysis of QSAA amplification products generated under optimized conditions (MM, SO_4^{2-}, 70°C). Two distinct morphologies were observed: densely packed fibrillar aggregates (top) and loosely associated fibrillar assemblies (bottom). Scale bars: 20 μm (left), 2 μm (right).

Figure 2

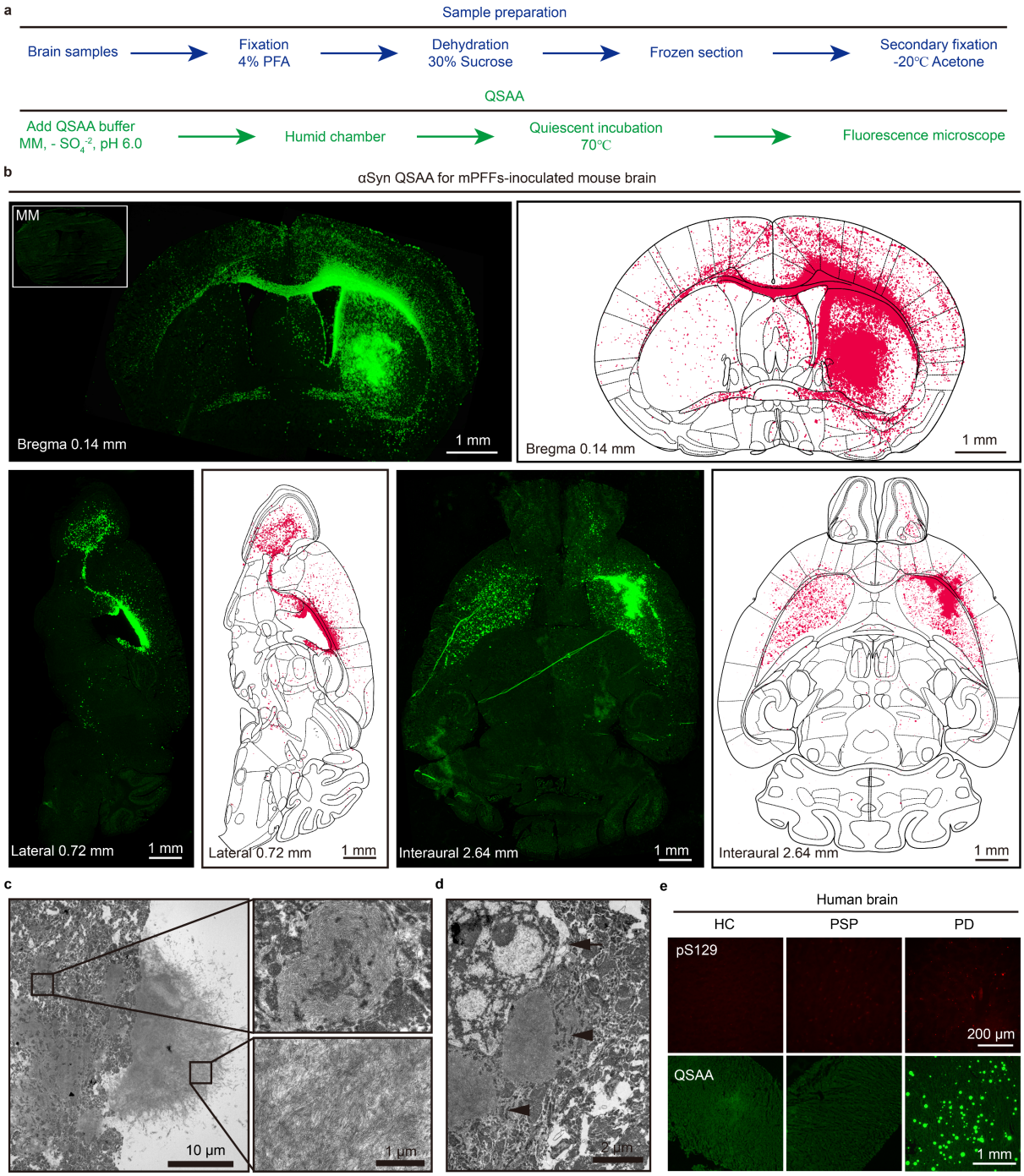

Figure 2. QSAA enables *in situ* amplification of pathological αSyn seeds in tissue sections. a, Schematic workflow of the QSAA procedure. **b,** Representative image of QSAA showed the distribution of αSyn seeds in coronal, sagittal, and horizontal sections of mouse brains, 90 days after intrastriatal mPFFs injection. The schematic diagrams on the right illustrate the distribution of ThT-positive signals, highlighted in red. Coordinates of the

mouse brain for each section were indicated (coronal: Bregma 0.14 mm; sagittal: Lateral 0.72 mm; horizontal: Interaural 2.64 mm). **c,** TEM images of QSAA amplification products in the brain of the aforementioned mice. Top row: Compact aggregates confined within interstitial spaces, with higher magnifications showing concentric ring-like arrangements incorporating cellular debris. Bottom row: Loosely organized aggregates extending across the tissue surface, with magnified images emphasizing the fibrillar structure of these radiating aggregates. Scale bars are indicated. **d,** TEM image revealed the droplet-like aggregates of different sizes clustered (arrowhead) around the nucleus (arrow). Scale bar: 3 μm. **e,** Representative images of brain sections from healthy controls (HC), progressive supranuclear palsy (PSP) patients, and PD patients, analyzed via IF for pS129-αSyn (top row, red) and QSAA (bottom row, green). Scale bars: 200 μm (pS129), 1 mm (QSAA).

Figure 3

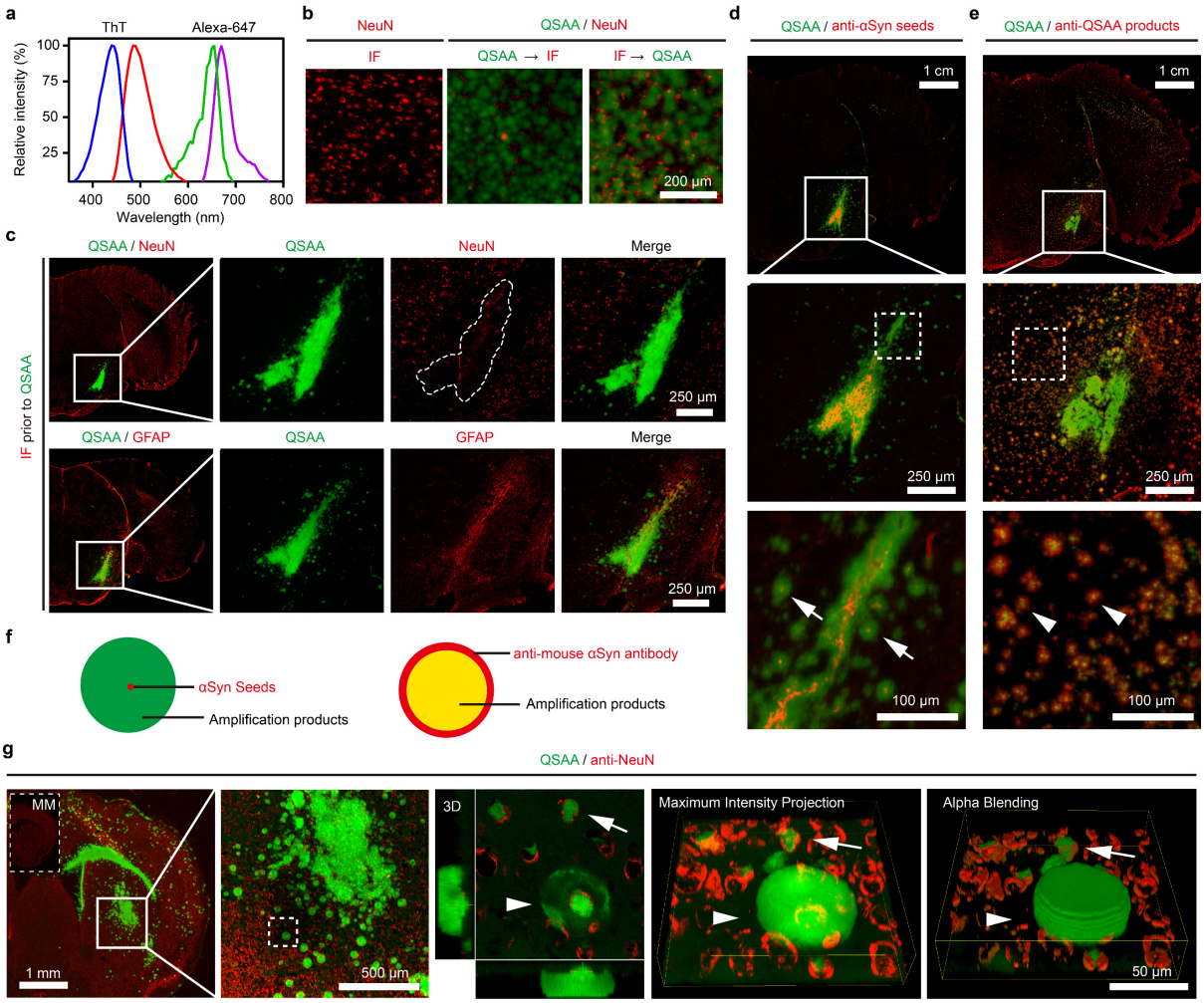

Figure 3. IF-QSAA: Visualize αSyn seeding with antibodies at the cellular level. a, Spectral profiles of ThT and Alexa Fluor 647. **b,** Representative images demonstrating the impact of the IF and QSAA order on signal detection. Performing IF after QSAA led to a significant loss of the NeuN signal (middle panel), whereas conducting IF before QSAA preserved both NeuN and ThT signals (right panel).Scale bar: 200 µm. **c,** Representative images of IF-QSAA in brain sections from mice injected with mPFFs into the SNc and sacrificed 90 days post-injection. The top row displays QSAA (green) combined with NeuN (red) staining, while the bottom row shows QSAA (green) combined with GFAP (red) staining. Scale bars: 250 µm. **d,** Brain sections were initially subjected to IF with a mouse-specific αSyn antibody (D37A6, red), followed by QSAA (green). The merged image

displays a "halo-like" pattern (arrows), with antibody-labeled aggregates at the core surrounded by QSAA products. Scale bars: 1 cm (top), 250 μm (middle), 100 μm (bottom). **e,** Brain sections were first treated with QSAA, followed by IF with the D37A6 antibody. The merged image showed that the newly formed QSAA products (green) were recognized by the anti-mouse αSyn antibody (red, arrowheads). Scale bars: 1 cm (top), 250 μm (middle), 100 μm (bottom). **f,** Schematic diagram on the left illustrating αSyn seeds (green) surrounded by amplification products (yellow). The right panel depicts the D37A6 antibody (red) recognized by the newly formed amplification products (yellow). **g,** High-resolution confocal microscopy images of IF-QSAA on brain sections from mice injected with mPFFs into the STR and euthanized 90 days post-injection. Sections were stained with NeuN (red) followed by QSAA (green). Some ThT signals were confined to the neurons (arrows), while others formed large aggregates, extending beyond the cellular boundaries (arrowheads). Control mice injected with mouse αSyn monomer (MM) showed only NeuN signals (left panel). Scale bars: 1 mm (left), 500 μm (middle), 50 μm (right).

Figure 4

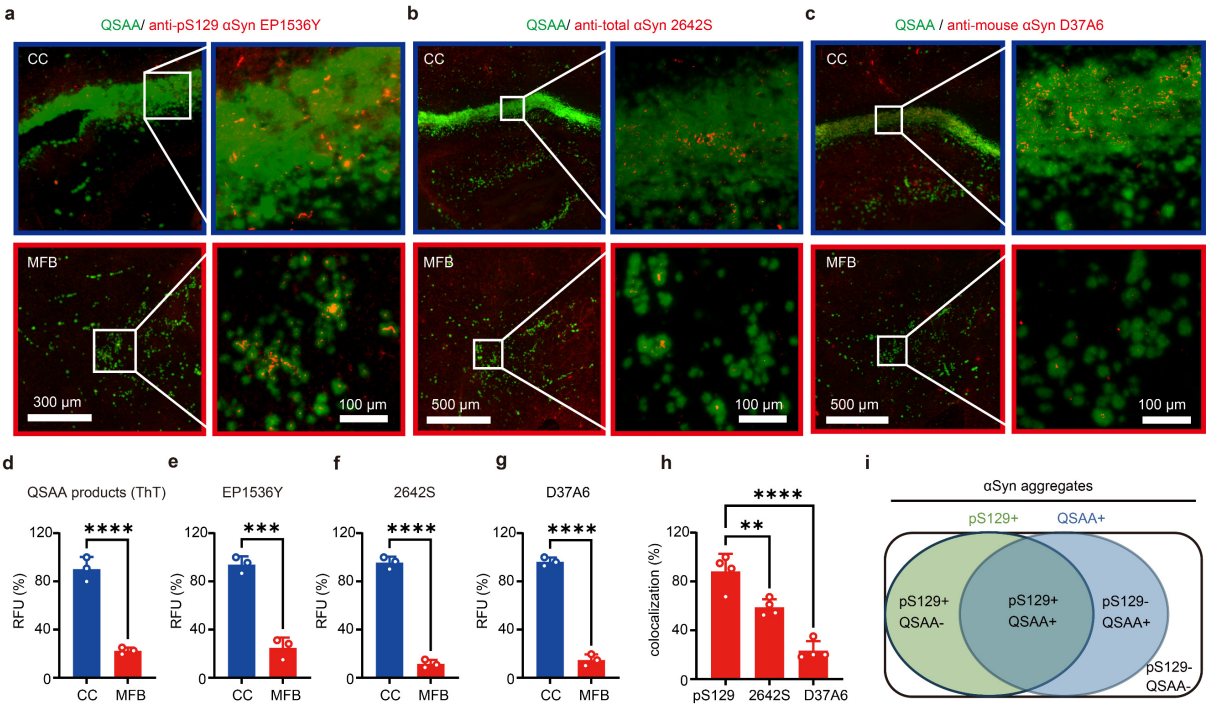

Figure 4. IF-QSAA reveals distinct distributions of αSyn aggregates and seeding activity. a-c, Representative images of IF-QSAA on brain sections from mice injected with mPFFs into the cortex, hippocampus, and substantia nigra, and sacrificed 6 months post-injection. Sections were subjected to IF using three different αSyn antibodies (red): (a) anti-pS129 αSyn (EP1536Y), (b) anti-total αSyn (2642S), and (c) anti-mouse αSyn (D37A6), followed by QSAA for 3h. Images depict two analyzed regions: the corpus callosum (CC, top row) and the medial forebrain bundle (MFB, bottom row). Scale bars are indicated. **d-g,** Quantification of the relative fluorescence intensity of QSAA (**d**) and the three antibodies: EP1536Y (**e**), 2642S (**f**), and D37A6 (**g**) in the CC and MFB. Data are presented as mean ± SD; ***$p < 0.001$; ****$p < 0.0001$. **h,** Quantification of amplification products of QSAA co-localized with each of the three antibodies in the MFB. Data are presented as mean ± SD; **$p < 0.01$, ****$p < 0.0001$. **i,** Schematic diagram illustrating the different states of pathological αSyn on the same slide, as revealed by IF-QSAA: pS129+/QSAA+ (αSyn aggregates with seeding activity), pS129+/QSAA- (αSyn aggregates without detectable seeding activity),

pS129-/QSAA+ (seeding activity without detectable pS129), and pS129-/QSAA- (no detectable signals in either assay).

Supplementary materials

Supplementary Figure 1

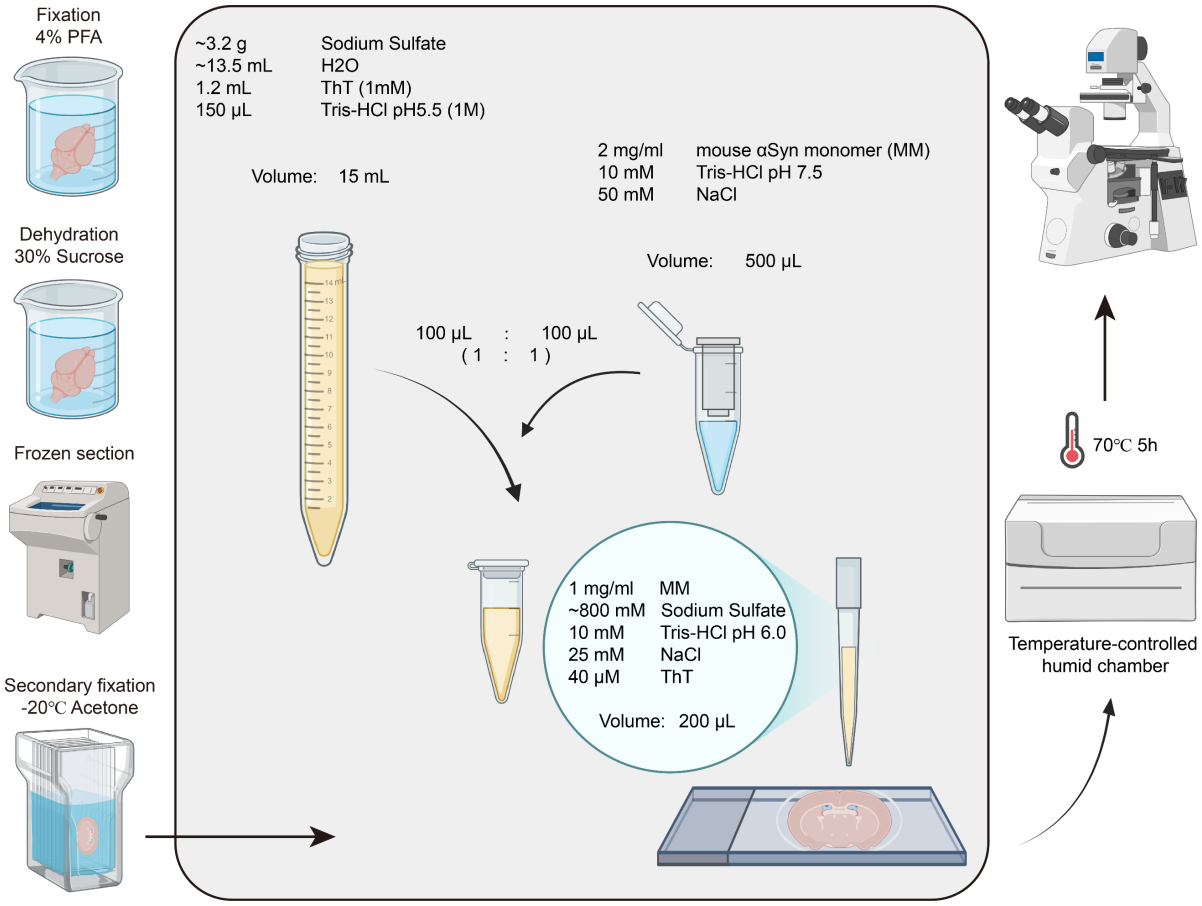

Supplementary Figure 1. Schematic workflow of the QSAA procedure. Fresh brain tissues were fixed in 4% PFA for 24 h, followed by dehydration in 30% sucrose solution for 48 h. Tissues were embedded in the OCT compound, and 14-µm-thick sections were cut and subjected to secondary fixation using acetone at -20°C for 10 min and air-dried. Sections were placed in a humid chamber and incubated with 200 µl QSAA buffer containing 1 mg/ml mouse αSyn monomer (MM), 800 mM sodium sulfate, 40 µM ThT, 25 mM NaCl, 10 mM Tris-HCl, at pH 6.0~6.5 at 70°C for 5 h. Fluorescence images were collected in the FITC channel through a fluorescence microscope

Supplementary Figure 2

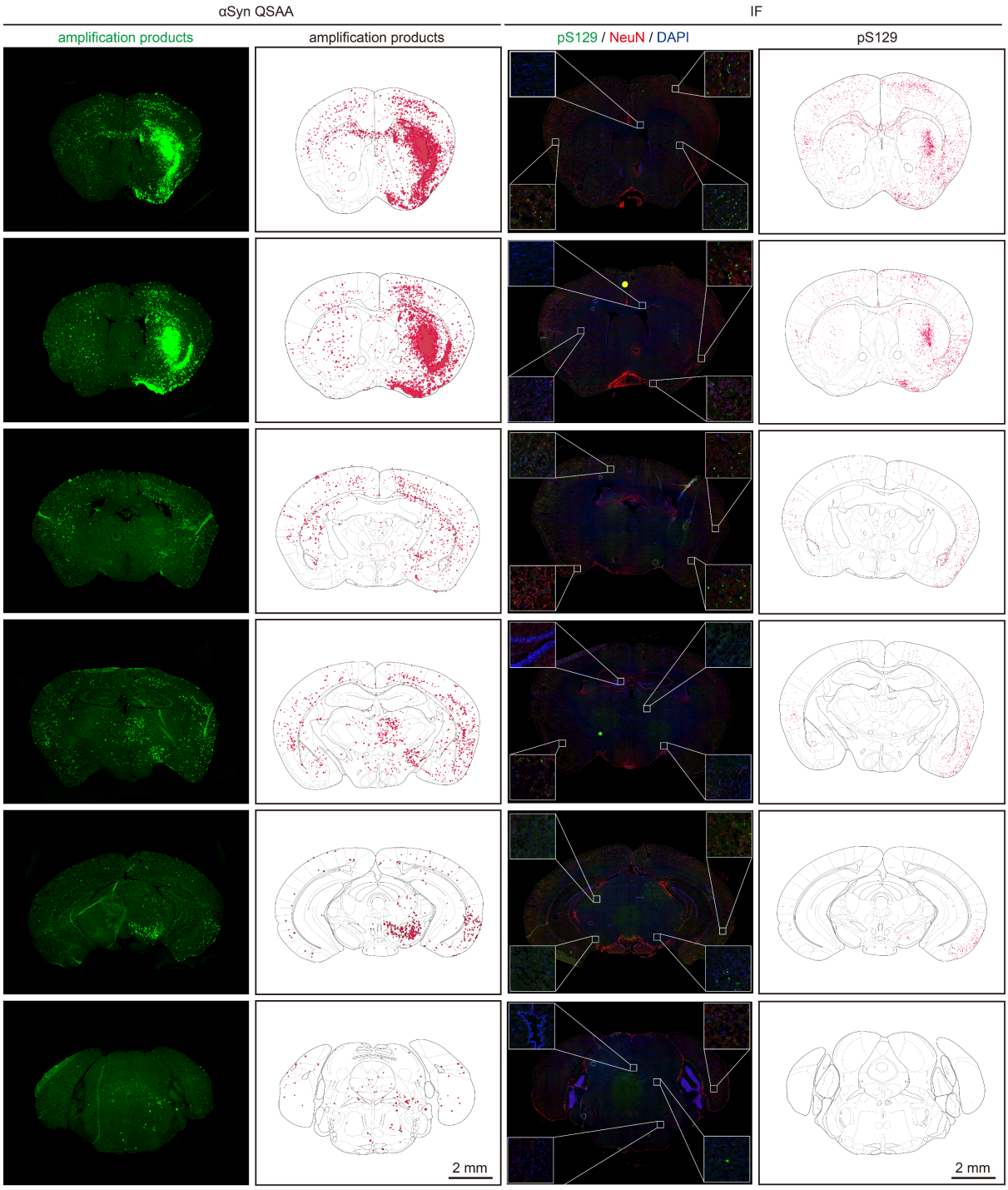

Supplementary Figure 2. Comparison of QSAA and pS129 in representing αSyn pathology in mPFF-inoculated mouse brain. Coronal brain sections from mice 6 months after mPFFs injection into the right striatum were analyzed using αSyn QSAA and IF. QSAA (left panels, green) revealed a widespread distribution of ThT-positive signals, indicative of

αSyn seed activity. The corresponding QSAA signals (red) are overlaid onto schematic representations of each coronal section (second column). Consecutive sections were stained using IF to detect pS129-αSyn immunoreactivity (red), along with NeuN (green) and DAPI (blue) staining (third column). Enlarged insets provided detailed views of pS129-αSyn localization. The anatomical distribution of pS129-αSyn was schematically represented in the fourth column (red). Rows are arranged along the anterior-posterior axis, from anterior (top) to posterior (bottom). Scale bars: 2 mm.

Supplementary Figure 3

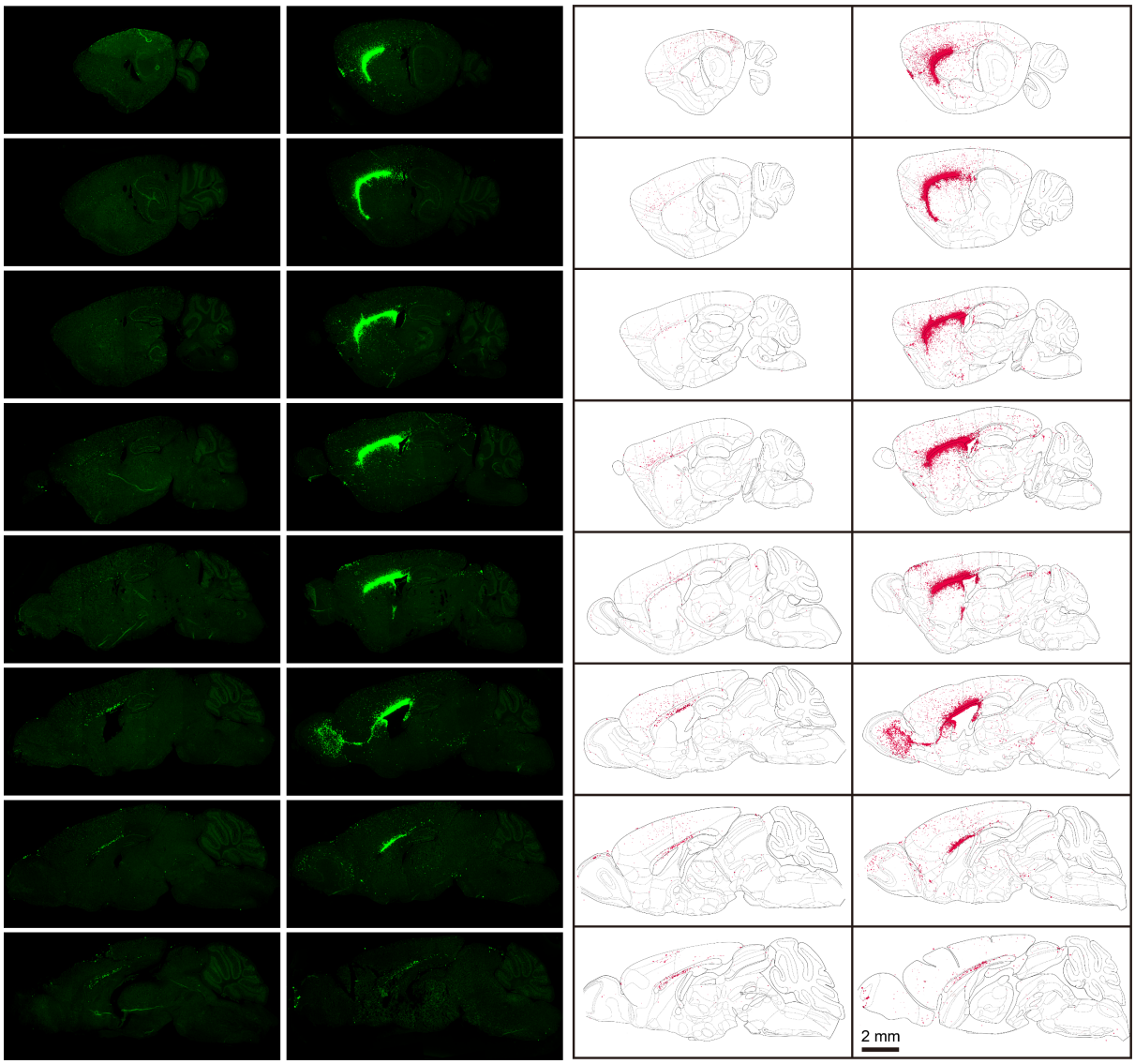

Supplementary Figure 3. Sagittal mapping of αSyn seeding activity in mPFF-inoculated mouse brain using QSAA. Left Panel: Representative sagittal brain sections from mice 6 months post mPFF-injection into the right striatum were analyzed using QSAA. Right Panel: The corresponding QSAA signals (red) are overlaid onto schematic representations of each sagittal section. Rows are arranged from lateral (top) to medial (bottom). Scale bars: 2 mm.

Supplementary Figure 4

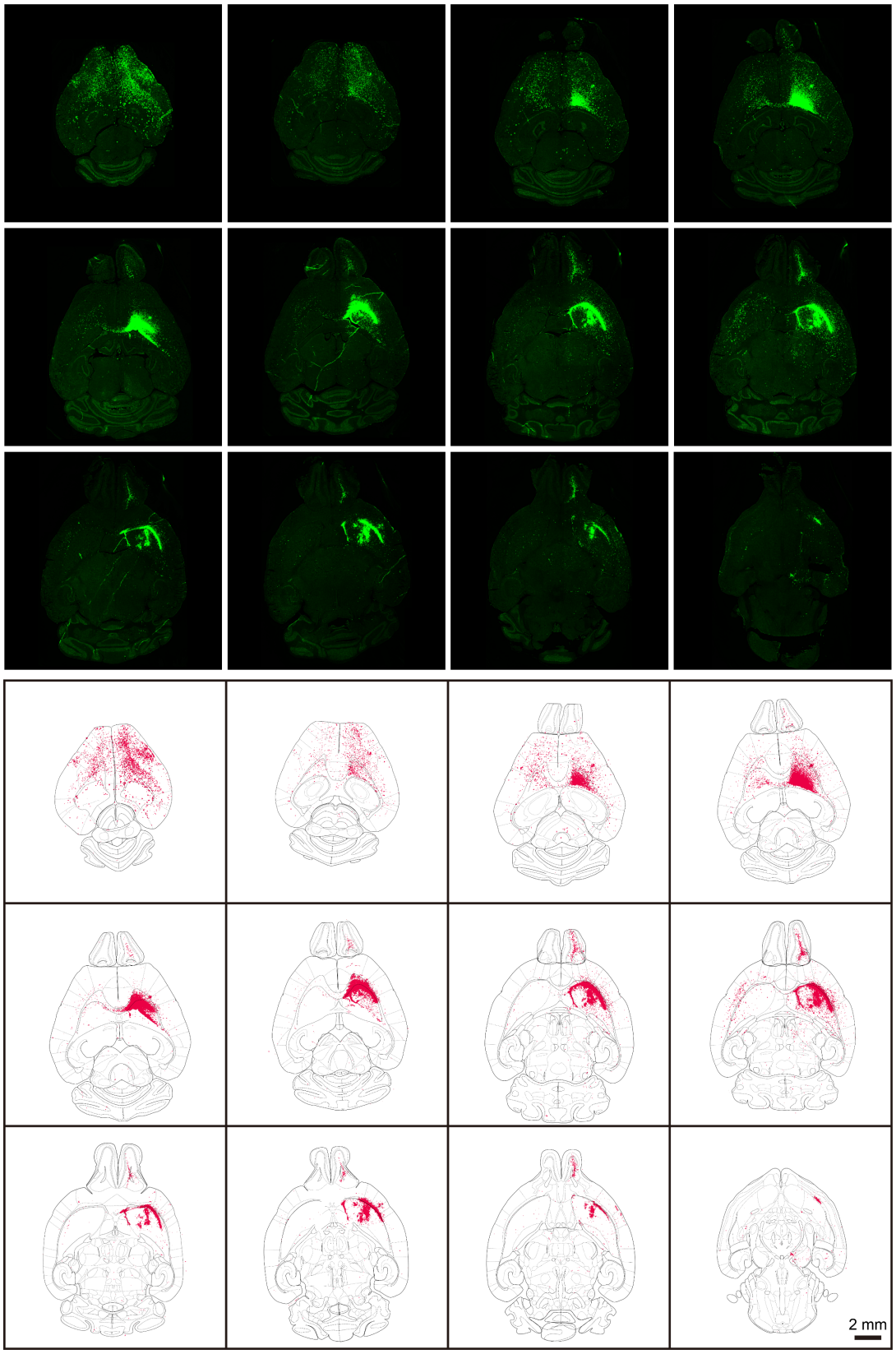

Supplementary Figure 4. Horizontal mapping of αSyn seeding activity in mPFF-inoculated mouse brain using QSAA. Representative horizontal brain sections from mice 6

months post mPFF-injection into the right striatum were analyzed using QSAA. The corresponding QSAA signals (red) are overlaid onto schematic representations of each horizontal section. Rows are arranged from dorsal (top) to ventral (bottom). Scale bars, 2 mm.